

Precision Spectroscopy of Atomic Hydrogen and Variations of Fundamental Constants

M. Fischer¹, N. Kolachevsky^{1,2}, M. Zimmermann¹, R. Holzwarth¹, Th. Udem¹, T.W. Hänsch^{1,3}, M. Abgrall⁴, J. Grünert⁴, I. Maksimovic⁴, S. Bize⁴, H. Marion⁴, F. Pereira Dos Santos⁴, P. Lemonde⁴, G. Santarelli⁴, P. Laurent⁴, A. Clairon⁴, and C. Salomon⁵

¹ Max-Planck-Institut für Quantenoptik, Hans-Kopfermann-Straße 1, 85748 Garching, Germany

² P.N. Lebedev Physics Institute, Moscow, Russia

³ Ludwig-Maximilians-University, Munich, Germany

⁴ BNM-SYRTE, Observatoire de Paris, 61 Avenue de l'Observatoire, 75014 Paris, France

⁵ Laboratoire Kastler Brossel, ENS, 24 rue Lhomond, 75005 Paris, France

Abstract. In 2003 we have measured the absolute frequency of the $(1S, F = 1, m_F = \pm 1) \rightarrow (2S, F' = 1, m'_F = \pm 1)$ two-photon transition in atomic hydrogen. By comparison with the earlier measurement in 1999 we can set an upper limit on its variation of (-29 ± 57) Hz within 44 months. We have combined this result with recently published results of optical transition frequency measurements in the $^{199}\text{Hg}^+$ ion and comparison between clocks based on ^{87}Rb and ^{133}Cs . From this combination we deduce the limits for fractional time variations of the fine structure constant $\dot{\alpha}/\alpha = \partial/\partial t(\ln \alpha) = (-0.9 \pm 2.9) \times 10^{-15} \text{ yr}^{-1}$ and for the ratio of ^{87}Rb and ^{133}Cs nuclear magnetic moments $\partial/\partial t(\ln[\mu_{\text{Rb}}/\mu_{\text{Cs}}]) = (-0.5 \pm 1.7) \times 10^{-15} \text{ yr}^{-1}$. This is the first precise restriction for the fractional time variation of α made without assumptions about the relative drifts of the constants of electromagnetic, strong and weak interactions.

1 Introduction

The question of constancy of fundamental constants was first raised in Dirac's "Large Number hypothesis" (1937) which aimed for a harmonization of basic laws of physics [1]. Since then, this hypothesis has been reviewed and extended by many other scientists opening a broad field of theoretical and experimental investigations. As there is no accepted theory predicting the values of fundamental constants, the question of their possible time variation belongs mostly to the field of experimental physics. The last decades saw a number of different astrophysical, geological, and laboratory tests searching for their possible variation in different time epochs with an ever increasing accuracy. From the point of view of its importance for physics in general, this problem stays at the same level as the test of *CPT*-symmetry and the search for an electric dipole moment of elementary particles.

In all metric theories of gravity including general relativity any drift of non-gravitational constants is forbidden. This statement bases on Einstein's Equiva-

lence Principle (EEP) postulating that (i) the weight of a body is proportional to its mass, (ii) the result of any non-gravitational measurement is independent of the velocity of the laboratory rest-frame (local Lorentz invariance), and (iii) the result of a non-gravitational measurement is independent of its time and position in this frame (local time and position invariance). On the other hand, theories towards a unified description of quantum mechanics and gravity allow for, or even predict some violations of EEP [2]. In this sense, any experimental search for a drift of fundamental constants tests the validity of EEP as well as it provides important constraints on new theoretical models.

The basic principle of all tests of the stability of fundamental constants is the investigation of time variations of some stable physical value Θ . Usually, Θ is a dimensionless value which can be the ratio of reaction cross-sections, the distances, masses, magnetic moments, frequencies and so on. In an experiment one measures the value Θ at two different times t_1 and t_2 and compares $\Theta(t_1)$ with $\Theta(t_2)$. The value of Θ may depend on a number of fundamental constants α_i ($i = 1, \dots, n$) and the conclusion about drifts of α_i originate from the analysis of $\Theta(t_1) - \Theta(t_2)$. The functional connection between Θ and α_i can include rather complicated theoretical models and assumptions which make the results somehow unclear and strongly model-dependent. Even if the dependence $\Theta(\alpha_i)$ is straightforward, it is difficult to separate the contributions from individual α_i drifts if $n > 1$. As mentioned in Ref. [3], all the relative drifts of fundamental constants, if existing, should be on the same order of magnitude which can result in a cancelation of the drift of Θ as well as in its amplification. For example, according to an elaborate scenario in the framework of a Grand Unification Theory, the fractional time variation of hadron masses and their magnetic moments should change about 38 times faster than the fractional time variation of the fine structure constant α [4].

Astrophysical and geological methods test the stability of fundamental constants over very long time intervals of 1–10 Gyr. Due to the large difference of $|t_1 - t_2|$, the sensitivity of these methods to a monotonic long-time drift is very high but they are insensitive to more rapid fluctuations. A recent analysis of quasar absorption spectra by Murphy *et al.* with redshifted UV transition lines indicates a variation of α on the level of $\Delta\alpha/\alpha = (-0.54 \pm 0.12) \times 10^{-5}$ in the first half of the evolution of the universe (5–11 Gyr ago) [5]. There are also indications that in this period the electron to proton mass ratio was different from its contemporary value on the same level of 10^{-5} [6]. The analysis of astrophysical data requires a number of model assumptions which include not only the well-established scenarios of the evolution of the universe, but also assumptions about the isotopic abundance in interstellar gas clouds, the presence of magnetic fields and others (see e.g. the review [7]) which are difficult to prove. More recent observation of quasar absorption spectra, performed by different groups, seem to rule out a variation of α on the level observed by Murphy *et al.* [8,9].

A very stringent limit for the time variation of α on geological timescales follows from the analysis of isotope abundance ratios in the natural fission reactor of Oklo, Gabon, which operated about 2 Gyr ago. A recent re-analysis of the data

of the $^{149}\text{Sm}/^{147}\text{Sm}$ isotope abundance ratio sets a limit of $\Delta\alpha/\alpha = (-0.36 \pm 1.44) \times 10^{-8}$ [10]. The interpretation of the data is not unambiguous, as the result strongly depends on reactor operating conditions which are not exactly known. Selecting another possible reaction branch yields a value of $\Delta\alpha/\alpha = (9.8 \pm 0.8) \times 10^{-8}$ [10]. In contrast to the first one, this result indicates a non-zero drift.

Laboratory experiments are sensitive to variations of fundamental constants during the last few years and typically base on precise frequency measurements in atomic or molecular systems. In comparison to astrophysical and geological ones, laboratory measurements considerably win in relative accuracy which, in spite of much shorter $|t_1 - t_2|$ time intervals, leads to a competitive sensitivity on drifts. Moreover, in this case systematic effects can be well controlled and the dependence of the transition frequencies on fundamental constants is straightforward.

Any absolute frequency measurement of some transition in an atomic system is a comparison of this frequency with the frequency of the ground state hyperfine transition of ^{133}Cs . Such a measurement of *one* transition frequency in *one* atomic system imposes a limit on the variation of some simple combinations of α , nuclear and electron magnetic moments and/or their masses [3]. To separate the drift of the fine-structure constant one needs either to impose some restricting assumptions on the time dependence of the coupling constants of the strong (α_S) and electroweak (α_W) interaction [4,11] or make absolute measurements of *two or more* transition frequencies possessing *different functional dependencies* on the fundamental constants. The second method does not include any model parameters or additional assumptions which favorably distinguishes it. It is also possible to make such a model-independent evaluation by directly comparing e.g. gross- and fine structure or two gross-structure frequencies without comparison to a primary frequency standard and thus excluding the corresponding dependence on the nuclear magnetic moments. To our knowledge, such laboratory experiments still have not been done with a level of accuracy competing modern absolute frequency measurements.

In this work we deduce separate stringent limits for the relative drifts of the fine structure constant α and the ratio μ_{Cs}/μ_B by combining the results of two optical frequency measurements in the hydrogen atom and in the mercury ion relative to the ground state hyperfine splitting of ^{133}Cs . The measurements of the hydrogen transition frequency have been carried out at MPQ, Garching, Germany and are described below. The experiments on the drift of the $5d^{10}6s\ ^2S_{1/2}(F=0) \rightarrow 5d^96s^2\ ^2D_{5/2}(F'=2, m'_F=0)$ electric quadrupole transition frequency ν_{Hg} in $^{199}\text{Hg}^+$ have been performed by the group of J. Bergquist at NIST, Boulder CO, USA between July 2000 and December 2002. They are described in detail elsewhere [12].

From 1999 to 2003, the ratio of the ground state hyperfine splittings of ^{87}Rb and ^{133}Cs has been determined from a comparison between several simultaneously running atomic fountain clocks in BNM-SYRTE and ENS, Paris, France

[13]. Using this result, we can also set a limit for the fractional time variation of the Rb and Cs nuclear magnetic moment ratio $\mu_{\text{Rb}}/\mu_{\text{Cs}}$.

As the measurements were performed at different places and at different times we have to use the hypothesis, that the results are independent of the place on the Earth's orbit, at least within the last 4 years. In other words, we have to assume a validity of local Lorentz invariance (LLI) and local position invariance (LPI) as well as to make the additional hypothesis, that the constants change on a cosmological time scale and do not oscillate within a few years (linear drifts). With this exceptions, our results are independent of any further model assumptions like any form of correlation between the constants or constancy of a particular set of constants.

2 Hydrogen spectrometer

In 1999 [14] and 2003, the frequency of the $(1S, F = 1, m_F = \pm 1) \rightarrow (2S, F' = 1, m'_F = \pm 1)$ two-photon transition in atomic hydrogen has been phase coherently compared to the frequency of the ground state hyperfine splitting in ^{133}Cs using a high-resolution hydrogen spectrometer and a frequency comb technique [15]. In 1999, the accuracy of the evaluation of the transition frequency was 1.8×10^{-14} . The setup of the hydrogen spectrometer used during this measurement has been described previously in [16]. We have introduced a number of

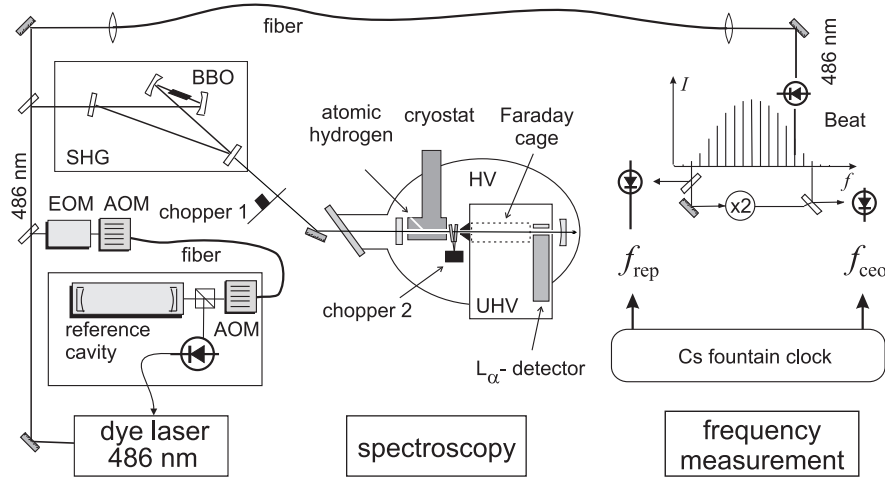


Fig. 1. Experimental setup for the comparison of the hydrogen $1S$ – $2S$ transition frequency with a primary frequency standard. The 486 nm light is doubled in a Barium β -Borate crystal (BBO) in the second harmonic generation (SHG) stage. Resulting radiation is coupled to a linear enhancement cavity in a vacuum chamber with the pressure of about 10^{-5} mbar (HV), while the excitation and detection take place in an ultra-high vacuum (UHV) zone at the pressure of 10^{-8} – 10^{-7} mbar. EOM and AOM denote electro- and acousto-optical modulators correspondingly.

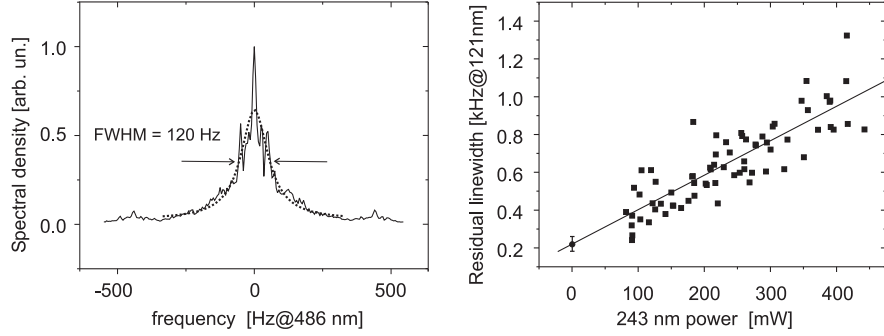


Fig. 2. (left) spectrum of the beat signal between laser fields locked to two independent cavities. (right) extrapolation of the ionization broadening of the $1S-2S$ transition spectra to zero excitation power circulating in the enhancement cavity.

improvements in the spectroscopic setup which will be described in the following. A sketch of the actual setup is shown in Fig.1.

A cw dye laser emitting near 486 nm is locked to an external reference cavity. The cavity used during the 1999 measurement was made from Zerodur and had a typical drift of 25 Hz s^{-1} at the fundamental frequency. The new cavity made from Ultra Low Expansion (ULE) glass for the 2003 measurement is better shielded against the environment. Its drift has been less than 0.5 Hz s^{-1} for the entire time of the measurement. Due to the better thermal and acoustic isolation and improvements in the laser locking electronics, the laser linewidth is narrower than it has been in 1999. An upper limit for the laser linewidth has been deduced from an investigation of the beat signal between two laser fields locked separately to independent Zerodur and ULE cavities. The spectrum of 12 averaged scans, each taken in 0.2 s is represented in Fig.2 (left). The width of this beat signal spectrum is about 120 Hz at a laser wavelength of 486 nm. Yet it is impossible to distinguish between the individual noise contributions from the two independent, but not equivalent cavities. Another restriction can be deduced from the analysis of the $1S-2S$ transition spectra. The linewidth of the transition is mainly defined by time-of-flight broadening and is between 1 kHz and 5 kHz at 121 nm. The residual linewidth obtained after subtracting the estimated contribution of time-of flight broadening is plotted on Fig.2 (right) versus the excitation light power. The observed broadening is due to the ionization processes and corresponds to a reduced lifetime of the metastable excited atoms. Extrapolating the residual linewidth to zero intensity, we get 240(30) Hz at 121 nm. This can be considered as a contribution from laser frequency fluctuations. Thus, we evaluate the 486 nm laser linewidth as 60 Hz for averaging times of 0.5 s.

A small part of the laser light is transferred to the neighboring laboratory via a single mode fiber where its absolute frequency can be measured. The main

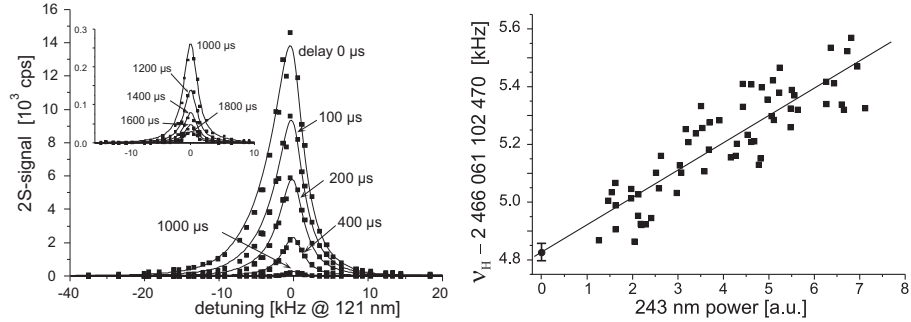


Fig. 3. (left) simultaneous fit of a $1S$ – $2S$ transition spectrum recorded at different delays Δt . The nozzle temperature was equal to 7 K. (right) AC Stark shift extrapolation.

part is frequency doubled in a BBO crystal. For higher conversion efficiency, the crystal is placed in a folded enhancement cavity. The resulting 20 mW of radiation near 243 nm (corresponding to half of the $1S$ – $2S$ transition frequency) is coupled into a linear enhancement cavity inside the vacuum chamber of the hydrogen spectrometer.

Molecular hydrogen is dissociated in a 15 W, 2.5 GHz radio-frequency gas discharge. The resulting flow of atomic hydrogen is cooled by inelastic collisions with the walls of a copper nozzle having the temperature of 5–7 K. The nozzle forms a beam of cold atomic hydrogen which leaves the nozzle collinearly with the cavity axis and enters the interaction region between the nozzle and the L_α -detector. This region is shielded from stray electric fields by a Faraday cage. Some of the atoms are excited from the ground state to the metastable $2S$ state by Doppler-free absorption of two counter-propagating photons from the laser field in the enhancement cavity. After the 1999 measurement which had been performed at a background gas pressure of around 10^{-6} mbar in the interaction region, we have upgraded the vacuum system to a differential pumping configuration. This allows us to vary the background gas pressure between 10^{-8} and 10^{-7} mbar in 2003 and to reduce the background gas pressure shift and the corresponding uncertainty down to 2 Hz.

Due to small apertures, only atoms flying close to the cavity axis can enter the detection region where the $2S$ atoms are quenched in a small electric field and emit L_α -photons. The excitation light and the hydrogen beam are periodically blocked by two phase locked choppers operating at 160 Hz frequency and the L_α -photons are counted time-resolved only in the dark period of the cycle. This eliminates background counts from the excitation light. The delay Δt between blocking the 243 nm radiation and the start of counting sets an upper limit on the velocity of the atoms which contribute to the signal. For some definite Δt only atoms with velocities $v < d/\Delta t$ are selected, where d is the distance between nozzle and detector. Therefore, velocity dependent systematic effects such as the second-order Doppler shift and the time-of-flight broadening are smaller for spectra recorded at larger Δt . The hydrogen beam is blocked by a fork chopper in less than 200 μs after the blocking of the excitation light to prevent slow

atoms from being blown away by fast atoms that emerge subsequently from the nozzle. With the help of a multi-channel scaler, we count all photons and sort them into 12 equidistant time bins. From each scan of the laser frequency over the hydrogen $1S-2S$ resonance we therefore get 12 spectra at different delays. To correct for the second order Doppler shift, we use an elaborated theoretical model [16] to fit all the delayed spectra of one scan simultaneously with one set of 7 fit parameters (see Fig.3). The result of the fitting procedure is the $1S-2S$ transition frequency for the hydrogen atom at rest.

Besides the second order Doppler effect, the other dominating systematic effect is the dynamic AC Stark shift which shifts the transition frequency linearly with the excitation light intensity. We have varied the intensity and extrapolate the transition frequency to zero intensity to correct for it [14]. A typical set of data taken within one day of measurement in 2003 and the corresponding extrapolation is presented in Fig.3 (right).

3 Frequency measurement

For an absolute measurement of the $1S-2S$ transition frequency in units of Hz, the frequency of the dye laser near 616.5 THz (486 nm) was phase coherently compared with a cesium fountain clock [13]. To bridge the large gap between the optical- and radio-frequency (RF) domain we took advantage of the recently developed femtosecond laser frequency comb technique incorporating a highly nonlinear glass fiber, which allows for a further simplification of the experimental setup as compared to the measurement performed in 1999. In this section we give an introduction of the frequency comb technique and a description of the experimental setup, which was used for $1S-2S$ frequency measurement in 2003.

The pulse train emitted by a sufficiently stable mode locked femtosecond (fs) laser equals a comb of cw laser modes in the frequency domain. The frequency of each mode of this comb can be written as $f_n = nf_{\text{rep}} + f_{\text{ceo}}$, where f_{rep} is the pulse repetition rate of the fs laser, n is an integer number and f_{ceo} is the so-called carrier envelope offset frequency [17].

The fs laser emits a train of pulses with a repetition rate $f_{\text{rep}} = 1/T$, where T is the time between consecutive pulses. The envelope function of the pulses has the periodicity of f_{rep} , but it does not necessarily mean that the electrical field of the pulses has the same periodicity. The pulses have identical field transients only when the laser cavity roundtrip phase delay of the fs laser pulse equals the group delay (Fig.4 top). In this case not only the envelope function but also the electrical field has the periodicity of f_{rep} . This leads to a Fourier spectrum $f_n = nf_{\text{rep}}$, where all the modes are exact multiples of f_{rep} . Generally, the group delay does not equal the phase delay inside the cavity and the frequencies f_n cannot be integer multiples of f_{rep} (Fig.4 bottom). Denoting the phase shift between the envelope function and the carrier frequency of consecutive pulses as $\Delta\varphi$ one can show, that the frequencies can be written as

$$f_n = nf_{\text{rep}} + f_{\text{ceo}} \quad \text{with} \quad (1)$$

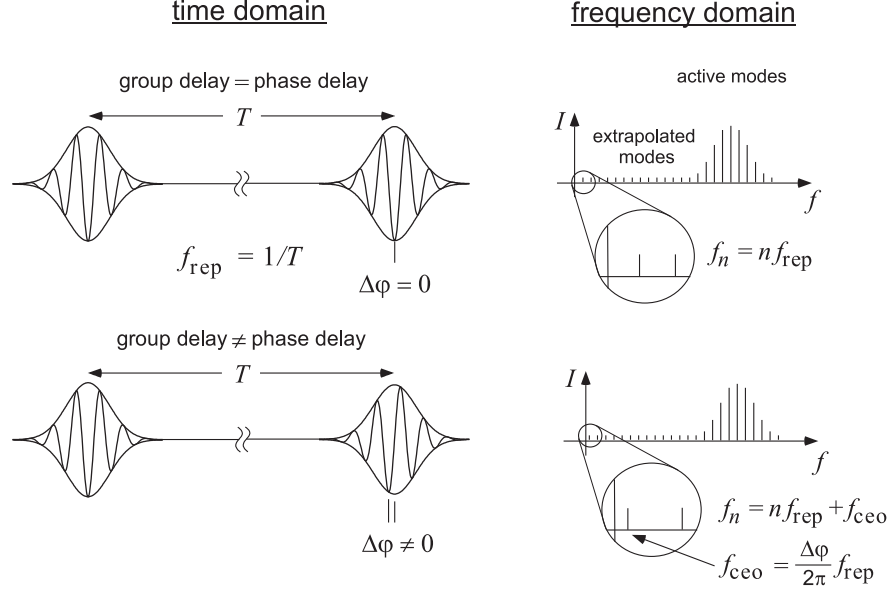
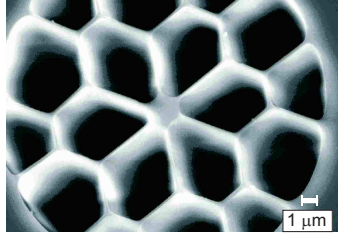


Fig. 4. Time- and frequency domain representation of a pulse train emitted by a mode-locked laser. If the phase delay is different from the group delay inside the laser cavity, this leads to the so-called carrier envelope offset frequency f_{ceo} , which shifts the frequency comb as a whole.

$$f_{\text{ceo}} = \frac{\Delta\varphi}{2\pi} f_{\text{rep}}, \quad f_{\text{ceo}} < f_{\text{rep}}.$$

If f_{rep} and f_{ceo} are fixed, all the modes of the frequency comb are determined in their frequency and can be used for measuring the frequency of cw laser light via beat notes between the cw laser light and a nearby comb mode. The large gap between the RF and the optical domain is bridged due to the fact that n is a large integer number of the order of 10^6 . To use the frequency comb for high precision optical frequency measurements one has to link f_{rep} and f_{ceo} phase coherently to a Cs primary frequency standard. The Cs clock provides us with an extremely precise reference frequency to control f_{rep} and f_{ceo} . The pulse repetition rate f_{rep} is easily measured with a photodiode and controlled via the length of the fs laser cavity, which can be changed by means of a piezo-mounted cavity mirror. In general, f_{ceo} can be controlled by adjusting the pump power of the fs laser [18,19]. In the case of a linear laser cavity with a prism pair to compensate for the group velocity dispersion, f_{ceo} can also be *controlled* by tilting the end mirror of the dispersive arm of the laser cavity [17]. The challenging problem for some time was to *measure* f_{ceo} . If the spectrum of the optical frequency comb covers an entire octave, f_{ceo} is most conveniently determined by frequency doubling the mode f_n on the low frequency side of the comb spectrum and comparing the result with the mode f_{2n} on the high frequency side via a beat note measurement [19,20]:

Core Design of a Photonic Crystal Fiber (PCF)



W. Wadworth, J. Knight, T. Birks, P. Russell
University of Bath, UK

Spectral Broadening of a fs Laser

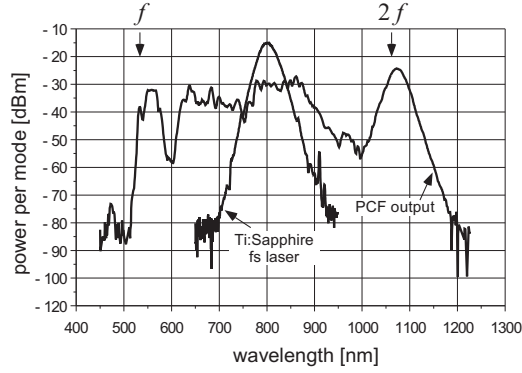


Fig. 5. Core design of a photonic crystal fiber (PCF) and spectral broadening of a fs laser. The PCF was seeded with 20 fs pulses and the average output power of the PCF was 180 mW.

$$2f_n - f_{2n} = 2(nf_{\text{rep}} + f_{\text{ceo}}) - (2nf_{\text{rep}} + f_{\text{ceo}}) = f_{\text{ceo}}. \quad (2)$$

If the spectrum does not cover an entire octave, one can alternatively compare $3.5f_{8n}$ and $4f_{7n}$ to get $\frac{1}{2}f_{\text{ceo}}$ [15,17] or $3f_{2n}$ with $2f_{3n}$ to obtain f_{ceo} [21–23]. The broad spectra needed for this technique are either directly emitted by the fs laser [24,25] or can be obtained by external broadening in a highly nonlinear medium such as a photonic crystal fiber (PCF) [26,27]. A PCF as pictured in Fig.5 can be designed to have zero group velocity dispersion (GVD) at 800 nm, which is the central wavelength of commonly used Ti:sapphire fs lasers. Due to the vanishing GVD the pulse spreading within the PCF is lower than in usual single mode fibers. The resulting high peak intensity leads to self phase modulation and therefore efficient broadening of the initial frequency comb.

If f_{rep} and f_{ceo} are stabilized by phase coherently linking them to a RF reference, the accuracy of the RF reference is in one step transferred to all cw modes of the octave spanning optical frequency comb. Using state-of-the-art Cs fountain clocks, which already reach accuracies of 10^{-15} [13], the frequency of an unknown light field can in principle be measured with the same level of accuracy. The fs frequency comb technique was tested to be accurate at the $< 10^{-16}$ level by comparing two independent systems [19,28]. To determine an optical frequency f_{opt} of the unknown light field one needs to measure the frequency f_{beat} of the beat note between the unknown light field and the neighboring mode f_n of the frequency comb. The unknown frequency f_{opt} can then be written as

$$f_{\text{opt}} = f_n + f_{\text{beat}} = nf_{\text{rep}} + f_{\text{ceo}} + f_{\text{beat}}. \quad (3)$$

The mode number n may be determined by a coarse measurement of f_{opt} with a commercial wavemeter. Using the fs frequency comb technique optical frequency

measurements have been carried out on atoms and ions, demonstrating accuracies of up to 10^{-14} [14,29–31]. An experimental setup for detecting f_{ceo} , f_{rep} and f_{beat} using an octave broad frequency comb is shown in Fig.6.

Another application of fs frequency combs is the determination of optical frequency ratios. As a frequency is dimensionless, no RF reference based on Cs is needed and one can take advantage of the high stability and accuracy of optical frequency standards, which should lead to an increased sensitivity to the drift of fundamental constants [31]. Due to the invention of photonic crystal fibers the complexity of the frequency measurement in 2003 has been considerably reduced as compared to the 1999 experiment, where a fs laser was already in use. The experimental setup used in 2003 to measure the frequency of the hydrogen spectroscopy dye laser was equivalent to that shown in Fig.6 and employed a fs Ti:sapphire ring laser (GigaOptics, model GigaJet) with 800 MHz repetition rate. The spectrum of the fs laser was externally broadened with the help of a PCF to more than one octave including light from 946 nm to 473 nm. The detection of the repetition rate f_{rep} was placed in front of the microstructured fiber to not be affected by amplitude noise caused by imperfect fiber coupling. f_{rep} was phase locked to a 800 MHz signal which was directly derived from the transportable Cs fountain clock FOM. For both the 1999 and 2003 measurements, the transportable Cs fountain clock FOM has been installed at MPQ. Its instability is $1.8 \times 10^{-13} \tau^{-1/2}$ and its accuracy has been evaluated to be 8×10^{-16} [32] at BNM-SYRTE. During the experiments in Garching, only a

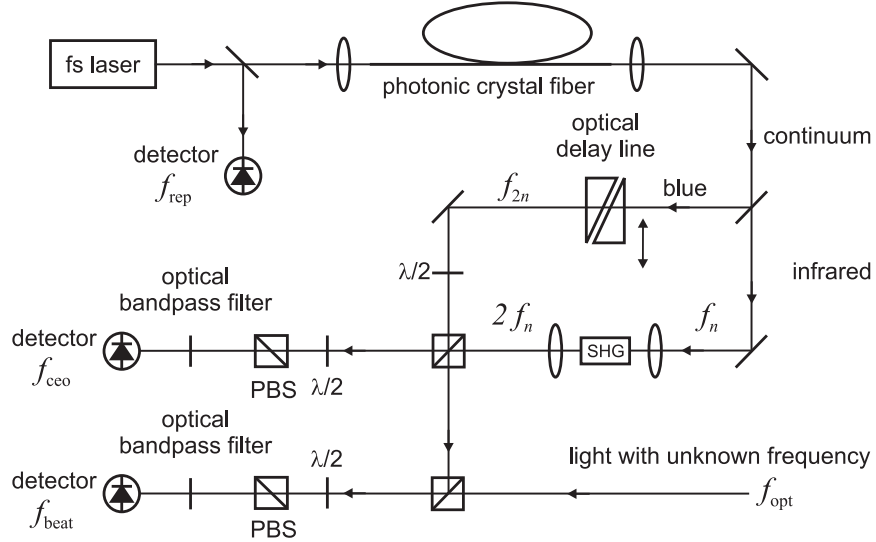


Fig. 6. Experimental setup for detecting f_{rep} , f_{ceo} and f_{beat} . An optical delay line is inserted into the “blue” arm of the nonlinear interferometer to match the optical path lengths. PBS denotes a polarizing beam splitter.

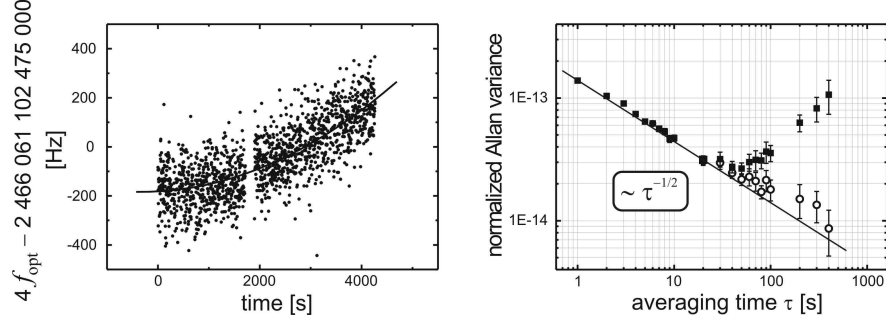


Fig. 7. (left) beat frequency of the 486 nm dye laser relative to the stabilized fs frequency comb. The solid line is a parabolic fit to the data. (right) normalized Allan variance vs. averaging time computed from a time series of 1 second counter readings with a considerable dead time. The straight line indicates the $\tau^{-1/2}$ dependence, which is the signature of the Cs fountain clock. The raw data analysis (squares) shows that the stability for averaging times longer than 20 s is limited by the drift of the ULE reference cavity. Open circles represent data corrected for the parabolic cavity drift.

verification at the level of 10^{-15} has been performed. Consequently we attribute a conservative FOM accuracy of 2×10^{-15} for these measurements.

To check for possible cycle slipping, the phase locked frequencies f_{ceo} and f_{rep} were additionally counted to verify consistency. The 486 nm dye laser and the blue part of the frequency comb were spatially overlapped, optically filtered around 486 nm, and directed onto an avalanche photodiode to measure the beat frequency with the neighboring mode of the frequency comb. The detected beat note was filtered, amplified and directed to three radio frequency counters (Hewlett Packard, models 53131A and 53132A) utilizing different detection bandwidth and power level. All counters were referenced to the Cs clock. To check for errors in the counting process only data points were accepted where all three counter readings were consistent with each other. Additionally it was verified that the dye laser was successfully locked to the ULE reference cavity during the measurement time.

Fig.7 shows a typical beat note measurement (left) and the corresponding normalized Allan variance (right) of the dye laser locked to the reference cavity relative to the fs frequency comb which was locked to FOM. For longer averaging times, the plot of the Allan variance is generated by juxtaposing 1-s counter readouts. Whereas it is known that such a procedure can alter the functional dependence of the Allan variance [33], white frequency noise, as produced by the Cs fountain, is immune to this form of bias. The observed $\tau^{-1/2}$ dependence coincides with the independently measured fountain clock instability for averaging times shorter than ≈ 10 s. The short term stability of the laser system is better than the stability of the fountain clock. However, the long term stability is limited by the drift of the ULE reference cavity.

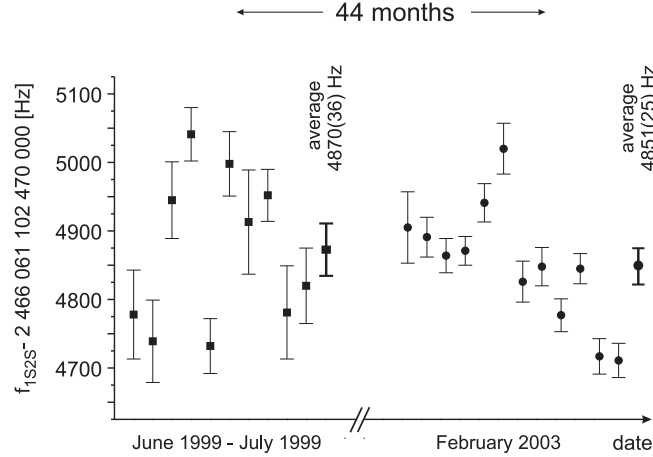


Fig. 8. Experimental results and averages for the 1999 and 2003 measurements of the $(1S, F = 1, m_F = \pm 1 \rightarrow 2S, F' = 1, m_F' = \pm 1)$ transition frequency in atomic hydrogen.

To compensate for the slow ULE cavity drift we fit a second-order polynomial to the measured beat note before averaging which significantly reduces the Allan variance for longer averaging times. To accurately determine the frequency of the dye laser, we first average the frequency of the ULE cavity with a polynomial such as the one shown on the left side of Fig. 6 with the consistent counter readout. Then we use this polynomial and the recorded AOM readings for each data point, that determine the cavity-laser detuning, to derive a highly stable value for the laser frequency. For the given stability of the Cs fountain clock and the cavity, the optimum record length is around 500 s. For longer averaging times the Cs fountain is more stable than the drift-corrected ULE cavity.

We have measured the $1S$ - $2S$ transition in atomic hydrogen during 10 days in 1999 and during 12 days in 2003. Both data sets have been analyzed using the same theoretical line shape model and are therefore comparable. In Fig. 8, the results of the extrapolation to zero excitation light intensity and the respective statistical error bars for each day are presented. Since 1999, the statistical uncertainty for each day of measurement was significantly reduced due to the narrower laser linewidth and better signal-to-noise ratio, but the scatter of the day averages did not reduce accordingly. We have tested several possible reasons for this additional scatter including an intra-beam pressure shift, a background gas pressure shift, Stark effects due to the RF gas discharge, and DC Stark shift and have been able to exclude all these effects at least on a conservative level of 10–20 Hz. A possible origin of the observed scatter can be due to a residual first order Doppler effect arising from a violation of the axial symmetry of the enhancement cavity mode and the hydrogen atomic beam. The scattering of the excitation light on intra-cavity diaphragms can also cause slight changes of the field distribution and the corresponding first order Doppler effect. However, it

Contribution	$\nu_{H,1999}$ [Hz]	$\sigma_{H,1999}$ [Hz]	$\nu_{H,2003}$ [Hz]	$\sigma_{H,2003}$ [Hz]
Extrapolated value – 2 466 061 102 474 kHz	870	36	851	25
Background gas pressure shift	10	10	0	2
Intra-beam pressure shift	0	10	0	10
Lineshape model	0	20	0	20
DC Stark shift	0	5	0	5
Blackbody radiation	0	1	0	1
Standing wave effects	0	10	0	1
Intensity zero uncertainty	0	1	0	0
Fountain clock uncertainty	0	5	0	5
Total – 2 466 061 102 474 kHz	880	45	851	34

Table 1. Results of the ($1S, F = 1, m_F = \pm 1 \rightarrow 2S, F' = 1, m'_F = \pm 1$) transition frequency measurement ($\nu_{H,1999}, \nu_{H,2003}$) and uncertainty budgets ($\sigma_{H,1999}, \sigma_{H,2003}$) for the 1999 and 2003 measurements correspondingly.

should average to zero over multiple adjustments of the hydrogen spectrometer because the shifts can have both signs. As the scatter is the same for both the measurement sets, we believe them to be equivalent. The main statistical and systematic uncertainties of these measurements are collected in Table 1. The averaging of the 1999 and 2003 daily data points was performed without weighting them.¹ For both measurements the dominating resulting uncertainty arises from the day-to-day scatter, while the pure statistical uncertainty for each day is significantly smaller. In fact, weighting of the day data only slightly influences the results (on the level of $\sigma/2$).

Comparing both measurements we deduce a difference of $\nu_{H,2003} - \nu_{H,1999}$ equal to (-29 ± 57) Hz within 44 months. This corresponds to a relative drift of ν_H against the ^{133}Cs ground state hyperfine splitting of $\partial_t(\ln(\nu_{\text{Cs}}/\nu_H)) = (3.2 \pm 6.3) \times 10^{-15}$ per year.

4 Determination of drift rates

Despite the high sensitivities (less than 10^{-14} yr^{-1}), the accuracy of transition frequency drift measurements are rather low (uncertainty is typically over 100%), so that only the first order expansion in terms of the constants involved in the evaluation is sufficient. The frequency of any optical transition can be written as

$$\nu = \text{const } Ry F_{\text{rel}}(\alpha), \quad (4)$$

where Ry is the Rydberg frequency expressed in Hertz and $F_{\text{rel}}(\alpha)$ takes into account relativistic and many-body effects. The Rydberg energy cancels in atomic

¹ The result of 2 466 061 102 474 870 Hz was inadvertently described in [14] as “the weighted mean value” but was calculated without consideration of the daily statistical uncertainties.

frequency comparisons. Therefore the dependence of Ry on α ($Ry \sim \alpha^2$) and other fundamental constants contained in Ry is irrelevant². The relativistic correction F_{rel} depends on the transition in the system considered and embodies additional dependence on α , while *const* is a numerical factor and is independent of any fundamental constants.

The frequency

$$\nu_{\text{Hg}} = 1\,064\,721\,609\,899\,143.7(10) \text{ Hz} \quad (5)$$

of the $5d^{10}6s^2 S_{1/2}(F=0) \rightarrow 5d^96s^2 {}^2D_{5/2}(F'=2, m'_F=0)$ electric quadrupole transition in $^{199}\text{Hg}^+$ was precisely measured at NIST between the years 2000 and 2002 [12]. Numerical calculations including relativistic and many-body effects for the dependence of $F_{\text{rel,Hg}}(\alpha)$ for ν_{Hg} on the fine structure constant α yield [34]

$$\alpha \frac{\partial}{\partial \alpha} \ln F_{\text{rel,Hg}}(\alpha) \approx -3.2. \quad (6)$$

In the light hydrogen atom, the relativistic correction for ν_{H} nearly vanishes ($F_{\text{rel,H}}(\alpha) \approx \text{const.}$):

$$\alpha \frac{\partial}{\partial \alpha} \ln F_{\text{rel,H}}(\alpha) \approx 0 \quad (7)$$

or

$$\nu_{\text{H}} \sim Ry. \quad (8)$$

The frequency of hyperfine transitions have a different functional dependence on α . For the ground state hyperfine transition in ^{133}Cs we have

$$\nu_{\text{Cs}} = \text{const}' Ry \alpha^2 \frac{\mu_{\text{Cs}}}{\mu_B} F_{\text{rel,Cs}}(\alpha) \quad (9)$$

with a relativistic correction $F_{\text{rel,Cs}}(\alpha)$ of [34]

$$\alpha \frac{\partial}{\partial \alpha} \ln F_{\text{rel,Cs}}(\alpha) \approx +0.8. \quad (10)$$

Combining these equations, we find that the comparison of the clock transition in Hg against a primary frequency standard tests the following fractional time variation [12]:

$$\begin{aligned} \frac{\partial}{\partial t} \ln \frac{\nu_{\text{Cs}}}{\nu_{\text{Hg}}} &= \frac{\partial}{\partial t} \ln \left(\frac{\alpha^2 \frac{\mu_{\text{Cs}}}{\mu_B} F_{\text{rel,Cs}}(\alpha)}{F_{\text{rel,Hg}}(\alpha)} \right) = 2 \frac{\partial \ln \alpha}{\partial t} + \frac{\partial}{\partial t} \ln \frac{\mu_{\text{Cs}}}{\mu_B} + (0.8 + 3.2) \frac{\partial \ln \alpha}{\partial t} \\ &= 6 \frac{\partial}{\partial t} \ln \alpha + \frac{\partial}{\partial t} \ln \frac{\mu_{\text{Cs}}}{\mu_B} = (0.2 \pm 7) \times 10^{-15} \text{ yr}^{-1} \end{aligned} \quad (11)$$

² The expansion of ν in terms of small changes of α as given in [34] are said to be derived assuming the constancy of the Rydberg frequency. However, no such restriction on the unit of frequency is necessary here, as any chosen unit will cancel out in the final result since only frequency ratios are used.

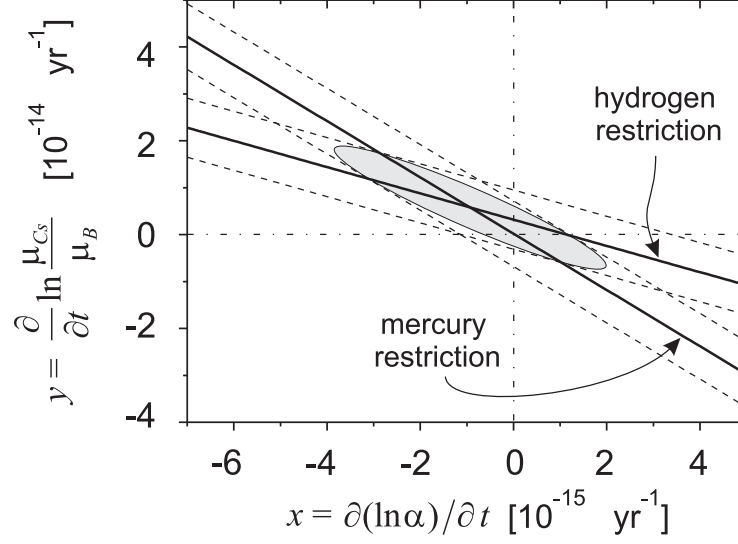


Fig. 9. Drifts of the $^2S_{1/2}(F=0) \rightarrow ^2D_{5/2}(F'=2, m'_F=0)$ transition in $^{199}\text{Hg}^+$ and of the $1S(F=1, m_F=\pm 1) \rightarrow 2S(F'=1, m'_F=\pm 1)$ transition in H against the frequency of the ground-state hyperfine transition in ^{133}Cs . Dashed lines represent 1σ experimental restrictions from the mean measured values. The elliptical region defined by $R(\Delta x, \Delta y) = 1$ gives the standard deviation for x and y when projected on corresponding axis by integration over the other.

Likewise we derive for the fractional variation of $\nu_{\text{Cs}}/\nu_{\text{H}}$ from the hydrogen $1S$ - $2S$ experiment [this work]:

$$\frac{\partial}{\partial t} \ln \frac{\nu_{\text{Cs}}}{\nu_{\text{H}}} = 2.8 \frac{\partial}{\partial t} \ln \alpha + \frac{\partial}{\partial t} \ln \frac{\mu_{\text{Cs}}}{\mu_{\text{B}}} = (3.2 \pm 6.3) \times 10^{-15} \text{ yr}^{-1} \quad (12)$$

With $x = \partial_t \ln \alpha$ and $y = \partial_t \ln(\mu_{\text{Cs}}/\mu_{\text{B}})$ we can write the experimental results as

$$6x + y = (0.2 \pm 7) \times 10^{-15} \text{ yr}^{-1} \quad (\text{Hg}^+), \quad (13)$$

$$2.8x + y = (3.2 \pm 6.3) \times 10^{-15} \text{ yr}^{-1} \quad (\text{H}). \quad (14)$$

These equations are easily solved, yielding the mean expectation values $\langle y \rangle$ and $\langle x \rangle$ without any assumptions of possible correlations between the drifts. In Fig. 9, both equations and the graphical solution are shown. Obviously, testing the stability of α by monitoring only one transition frequency during a time period would require additional assumptions of the drift of other fundamental constants.

The uncertainties can be calculated by making two assumptions: (i) the experimental data are Gaussian distributed and (ii) the mercury (13) and the hydrogen (14) measurements are statistically independent. In this case normal

gaussian error propagation allows the calculation of the variances $\langle y^2 \rangle - \langle y \rangle^2$ and $\langle x^2 \rangle - \langle x \rangle^2$ even when the drift rates x and y are correlated [4]. This is because the covariance term $\langle xy \rangle$ does not appear when (13,14) are resolved for x and y .

For a graphical representation it is possible to calculate the two-dimensional probability density of x and y to be the true values:

$$P(x, y) = \frac{1}{2\pi\sqrt{\sigma_H \sigma_{Hg}}} \exp[-R(\Delta x, \Delta y)/2], \quad (15)$$

where Δx and Δy are the distances along the corresponding axes from the crossing point of the solid lines (Fig.9) i.e. the solution of (13,14). The experimental uncertainties are $\sigma_H = 6.3 \times 10^{-15} \text{ yr}^{-1}$ and $\sigma_{Hg} = 7 \times 10^{-15} \text{ yr}^{-1}$ taken from (13) and (14), and the exponent function is given by:

$$R(\Delta x, \Delta y) = (\Delta y + 6\Delta x)^2 / \sigma_{Hg}^2 + (\Delta y + 2.8\Delta x)^2 / \sigma_H^2. \quad (16)$$

We deduce the uncertainties for x and y as projections of the ellipse defined by $R(\Delta x, \Delta y) = 1$ on the corresponding axes (Fig.9) by integration over the other dimension. For only two independent measurements this method is equivalent to performing simple Gaussian error propagation of uncertainties when resolving (13,14). However, the projection method can be generalized to more than two measurements, i.e. more than two equations for the two unknowns x and y (see contribution by E. Peik in this volume). The integration in both directions can be performed analytically to derive the uncertainties of x and y . Our evaluation is model-independent in the sense that we neither assume x and y to be uncorrelated nor that they are correlated in any way.

The relative drift of the fine structure constant α between July 2000 and the end of 2003 is

$$x = \frac{\partial}{\partial t} \ln \alpha = (-0.9 \pm 2.9) \times 10^{-15} \text{ yr}^{-1}. \quad (17)$$

For the limit on the relative drift of μ_{Cs}/μ_B , we find

$$y = \frac{\partial}{\partial t} \ln \frac{\mu_{Cs}}{\mu_B} = (0.6 \pm 1.3) \times 10^{-14} \text{ yr}^{-1}. \quad (18)$$

The given 1σ uncertainties for x and y incorporate both the statistical and systematic uncertainties of the hydrogen and the mercury measurements. Both limits (17) and (18) are consistent with zero.

These results allow us to deduce a restriction for the relative drift of the ratio of the nuclear magnetic moments in ^{87}Rb and ^{133}Cs . From 1998 to 2003, the drift of the ratio of the ground state hyperfine frequencies in ^{87}Rb and ^{133}Cs has been measured to be [13]

$$\frac{\partial}{\partial t} \ln \frac{\nu_{\text{Rb}}}{\nu_{\text{Cs}}} = (0.2 \pm 7.0) \times 10^{-16} \text{ yr}^{-1}. \quad (19)$$

Substituting the corresponding dependencies $F_{\text{rel}}(\alpha)$ for these transitions [13,34], we can write

$$\frac{\partial}{\partial t} \ln \frac{\nu_{\text{Rb}}}{\nu_{\text{Cs}}} = \frac{\partial}{\partial t} \left(\ln \frac{\mu_{\text{Rb}}}{\mu_{\text{Cs}}} - 0.53 \ln \alpha \right). \quad (20)$$

Combining (17), (19), and (20) we deduce a restriction for the relative drift of the nuclear magnetic moments in ^{87}Rb and ^{133}Cs :

$$\frac{\partial}{\partial t} \ln \frac{\mu_{\text{Rb}}}{\mu_{\text{Cs}}} = (-0.5 \pm 1.7) \times 10^{-15} \text{ yr}^{-1}. \quad (21)$$

where the same procedure as in Fig.9 was used with a diagram covering x and $z = \partial_t \ln(\mu_{\text{Rb}}/\mu_{\text{Cs}})$.

The values of the nuclear moments are determined by the strong and the electromagnetic interaction. If the former is constant, the time changing nuclear moments point toward a variation of the strong coupling constant. Unfortunately, there is no simple scaling law such as (4) or (9) known for the nuclear moments. However, they can be approximated with the Schmidt model [35]. For ^{87}Rb and ^{133}Cs atoms the Schmidt nuclear magnetic moments μ^s depend only on the proton gyromagnetic ratio g_p . Using this model, one can get an approximate relation

$$\frac{\partial}{\partial \ln g_p} \ln \frac{\mu_{\text{Rb}}^s}{\mu_{\text{Cs}}^s} \simeq 2, \quad (22)$$

which, in combination with (21), yields a stringent upper bound for the drift of the proton gyromagnetic factor g_p :

$$\frac{\partial}{\partial t} \ln g_p = (-0.2 \pm 0.8) \times 10^{-15} \text{ yr}^{-1}. \quad (23)$$

5 Conclusion

In conclusion, we have determined limits for the drift of α , μ_{Cs}/μ_B and $\mu_{\text{Rb}}/\mu_{\text{Cs}}$ from laboratory experiments without any assumptions of their conceivable correlations. All these limits are consistent with zero drift. Table 2 represents some of the most accurate recent measurements of drifts of the fine structure constant α in different epochs. From all these data only the investigations of quasar absorption spectra measured with the Keck/HIRES spectrograph show a significant deviation between the values of α today and 10 Gyrs ago [5]. Considering the Oklo data as well as results of modern astrophysical and laboratory measurements one can suppose that the drift, if existent at all, is not linear and that α has reached an asymptotic value or is in the extremum of an oscillation or is simply too small to be detected yet. To make a definite conclusion additional independent astrophysical data as well as a further increase of the accuracy of laboratory methods are required.

6 Acknowledgements

We thank S.G. Karshenboim for the fruitful discussion of this work. N. Kolachevsky acknowledges support from Alexander von Humboldt Stiftung. The work was partly supported by the Deutsche Forschungsgemeinschaft (grant No.

Method, reference	$t_2 - t_1$	$[\alpha(t_1) - \alpha(t_2)]/\alpha$	Model assumptions
Geological (Oklo reactor) [10]	2 Gyr	$(-0.36 \pm 1.44) \times 10^{-8}$	fission conditions, $\dot{\alpha}_S = \dot{\alpha}_W = 0$
Astrophysical (absorption spectra) [5]	5–11 Gyr	$(-0.54 \pm 0.12) \times 10^{-5}$	astrophysical models
Astrophysical (absorption spectra) [8]	9.7 Gyr	$(-0.06 \pm 0.06) \times 10^{-5}$	astrophysical models
Astrophysical (absorption spectra) [9]	8 Gyr	$(0.1 \pm 1.7) \times 10^{-5}$	astrophysical models
Laboratory (Rb–Cs clocks comparison) [13]	4 yr	$(0.2 \pm 5.2) \times 10^{-15}$	$\dot{\alpha}_S = \dot{\alpha}_W = 0$
Laboratory (Hg ⁺ transition frequency measurement) [12]	3 yr	$(-0.1 \pm 3.5) \times 10^{-15}$	$\dot{\alpha}_S = \dot{\alpha}_W = 0$
Laboratory (H transition frequency measurement) [this work]	3.6 yr	$(-4.1 \pm 8.2) \times 10^{-15}$	$\dot{\alpha}_S = \dot{\alpha}_W = 0$
Combination of [12] and this work	3.5 yr	$(3.2 \pm 10.2) \times 10^{-15}$	LLI, LPI, linear drifts

Table 2. Some of the precise recent measurements testing the relative changes of the fine-structure constant α over a time interval $(t_2 - t_1)$ where t_2 is the present time and t_1 corresponds to the past. The drift can be calculated as $\partial/\partial t(\ln \alpha) \simeq [\alpha(t_2) - \alpha(t_1)] \alpha^{-1} (t_2 - t_1)^{-1}$. Combining the results of absolute frequency measurements of the optical transitions in Hg⁺ and H yields a restriction for the drift of α without assumptions of conceivable correlations between the constants.

436RUS113/769/0-1) and RFBR. The development of the FOM fountain was supported by Centre National d’études spatiales and Bureau National de Métrologie.

References

1. P.A.M. Dirac, *Nature* (London) **139**, 323 (1937).
2. T. Damour and A.M. Polyakov, *Nucl. Phys. B* **423**, 532 (1994).
3. S.G. Karshenboim, physics/0306180.
4. X. Calmet, H. Fritzsch, *Eur. Phys. J. C* **24**, 639 (2002).
5. M. T. Murphy, J. K. Webb, V. V. Flambaum, astro-ph/0306483, see also J. K. Webb *et al.*, *Phys. Rev. Lett* **87**, 091301 (2001).
6. A. Ivanchik, P. Petitjean, E. Rodriguez, and D. Varshalovich, astro-ph/0210299.
A. Ivanchik, A. Potekhin, and D. Varshalovich, *Astron. and Astroph.* **343**, 439 (1999).
7. J.-P. Uzan, *Rev. Mod. Phys.* **75**, 403 (2003).
8. H. Chand, R. Srianand, P. Petitjean, and B. Aracil, *Astron. and Astroph.* **417**, 853 (2004).

9. R. Quast, D. Reimers, and S.A. Levshakov, *Astron. and Astroph.* **415**, 27 (2004).
10. Y. Fujii, *et al.*, *Nucl. Phys. B*, **573**, 377 (2000).
11. J.D. Prestage, R.L. Tjoelker and L. Maleki, *Phys. Rev. Lett.* **74**, 3511 (1995).
12. S. Bize *et al.*, *Phys. Rev. Lett.* **90**, 150802 (2003).
13. H. Marion *et al.*, *Phys. Rev. Lett.* **90**, 150801 (2003).
14. M. Niering *et al.*, *Phys. Rev. Lett.* **84**, 5496 (2000).
15. J. Reichert *et al.*, *Phys. Rev. Lett.* **84**, 3232 (2000).
16. A. Huber *et al.*, *Phys. Rev. A* **59**, 1844 (1999).
17. J. Reichert, R. Holzwarth, Th. Udem and T.W. Hansch, *Opt. Commun.* **172**, 59 (1999).
18. H.A. Haus and E.P. Ippen, *Opt. Lett.* **26**, 1654 (2001).
19. R. Holzwarth *et al.*, *Phys. Rev. Lett.* **85**, 2264 (2000).
20. S.A. Diddams *et al.*, *Phys. Rev. Lett.* **84**, 5102 (2000).
21. T.M. Rammond, S.A. Diddams, L. Hollberg and A. Bartels, *Opt. Lett.* **27**, 1842 (2002).
22. U. Morgner *et al.*, *Phys. Rev. Lett.* **86**, 5462 (2001).
23. T.M. Fortier, D.J. Jones and S.T. Cundiff, *Opt. Lett.* **28**, 2198 (2003).
24. A. Bartels and H. Kurz, *Opt. Lett.* **27**, 1839 (2002).
25. R. Ell *et al.*, *Opt. Lett.* **26**, 373 (2001).
26. J.C. Knight, T.A. Birks, P.St.J. Russell and D.M. Atkin, *Opt. Lett.* **21**, 1547 (1996).
27. J.K. Ranka, R.S. Windeler and A.J. Stentz, *Opt. Lett.* **25**, 25 (2000).
28. S.A. Diddams, L. Hollberg, L.-Sh. Ma and L. Robertsson, *Opt. Lett.* **27**, 58 (2002).
29. Th. Udem *et al.*, *Phys. Rev. Lett.* **86**, 4996 (2001).
30. M. Eichenseer, A.Yu. Nevsky, Ch. Schwedes, J. von Zanthier and H. Walther, *J. Phys. B: At. Mol. Opt. Phys.* **36**, 553 (2003).
31. J. Stenger, H. Schnatz, C. Tamm and H. Telle, *Phys. Rev. Lett.* **88**, 073601 (2002).
32. M. Abgrall, Thèse de doctorat de l'université Paris VI (2003).
33. P. Lesage, *IEEE Trans. Instrum. Meas.* **32**, 204 (1983).
34. V.A. Dzuba, V.V. Flambaum, and J.K. Webb, *Phys. Rev. A* **59**, 230 (1999);
V.V. Flambaum, physics/0302015.
35. S. G. Karshenboim, *Can. J. Phys.* **78**, 639 (2000).